Article

Studying and Switching Electron Transfer: From the Ensemble to the Single Molecule

Michael W. Holman, Ruchuan Liu, Ling Zang, Ping Yan, Sara A. DiBenedetto, Robert D. Bowers, and David M. Adams

J. Am. Chem. Soc., **2004**, 126 (49), 16126-16133• DOI: 10.1021/ja047386o • Publication Date (Web): 17 November 2004

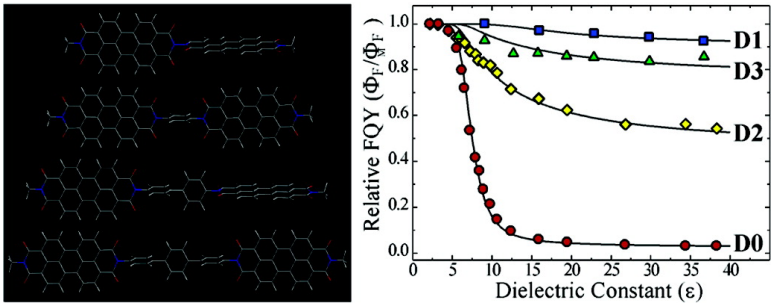

More About This Article

Additional resources and features associated with this article are available within the HTML version:

- Supporting Information
- Links to the 8 articles that cite this article, as of the time of this article download
- Access to high resolution figures
- Links to articles and content related to this article
- Copyright permission to reproduce figures and/or text from this article

View the Full Text HTML

J|A|C|S
ARTICLES
Published on Web 11/17/2004

Studying and Switching Electron Transfer: From the Ensemble to the Single Molecule

Michael W. Holman, Ruchuan Liu, Ling Zang,† Ping Yan, Sara A. DiBenedetto, Robert D. Bowers, and David M. Adams*

Contribution from the Department of Chemistry, Columbia University, 3000 Broadway, New York, New York 10027

Received May 4, 2004; E-mail: dadams@chem.columbia.edu

Abstract: We report here on the systematic investigation of photoinduced intramolecular electron transfer (IET) in a series of donor−bridge−acceptor molecules as a means of understanding electron transport through the bridge. Perylenebisimide chromophores connected by various oligophenylene bridges are studied because their electron-transfer behavior can readily be monitored by following changes in the fluorescence intensity. We find dramatic switching of the IET behavior as the solvent polarity (dielectric constant) is increased. By combining steady-state and time-resolved fluorescence spectroscopy in a variety of solvents at multiple temperatures with standard theories of electron transfer, we determine parameters governing the IET behavior of these dimers, such as the electronic coupling through the bridges. We also deploy available ab initio quantum chemical methods to calculate the through-space component of the electronic coupling matrix element. Single-molecule investigations of the electron-transfer behavior also show that IET can be switched *reversibly* by a similar mechanism in an isolated individual molecule.

Interest in the possibilities of molecular electronics[1−5] has led many researchers in recent years to pursue studies of the conductance of single-molecular wires.[6−9] Direct current/voltage measurements, in a break junction,[10,11] a scanning tunneling microscope,[12,13] or a conducting atomic force microscope,[14] can provide information about the conductivity of molecular wires, but measurements and their interpretation are often complicated by issues of molecular structure and dynamics, and of achieving and understanding the molecule−metal contact.[4,7] These methodologies also suffer from difficulties associated with measurement reproducibility, device fabrication, and low device yields. There is a need for alternate experimental approaches and methodologies which allow for the rapid determination of the properties of potential molecular electronic wires, structures, and devices.

Spectroscopic investigations of intramolecular electron transfer (IET) in donor−bridge−acceptor systems,[15−20] where the electrocontact is guaranteed by covalent bonding, offer an effective way to probe molecular electronic properties that are relevant to conduction, such as energy levels of molecular orbitals, and electronic coupling between different parts of a molecule. The electron-transfer theory for these systems,[21−23] built on the early work of Marcus,[24] allows these fundamental parameters to be estimated using rates constants measured by steady-state or time-resolved spectroscopies. Moreover, fluorescence spectroscopy can now be extended down to the single-molecule level[25−28] to follow the behavior of single molecules in unique nanoenvironments, and recently several groups have

† Present address: Department of Chemistry and Biochemistry, Southern Illinois University, Carbondale, IL 62901.

(1) Joachim, C.; Gimzewski, J. K.; Aviram, A. *Nature* **2000**, *408*, 541−8.
(2) Tour, J. M. *Acc. Chem. Res.* **2000**, *33*, 791−804.
(3) Carroll, R. L.; Gorman, C. B. *Angew. Chem., Int. Ed.* **2002**, *41*, 4378−4400.
(4) Cahen, D.; Hodes, G. *Adv. Mater.* **2002**, *14*, 789−98.
(5) Adams, D. M.; Brus, L.; Chidsey, C. E. D.; Creager, S.; Creutz, C.; Kagan, C. R.; Kamat, P. V.; Lieberman, M.; Lindsay, S.; Marcus, R. A.; Metzger, R. M.; Michel-Beyerle, M. E.; Miller, J. R.; Newton, M. D.; Rolison, D. R.; Sankey, O.; Schanze, K. S.; Yardley, J.; Zhu, X. *J. Phys. Chem. B* **2003**, *107*, 6668−6907.
(6) Nitzan, A.; Ratner, M. A. *Science* **2003**, *300*, 1384−1389.
(7) Mantooth, B. A.; Weiss, P. A. *Proc. IEEE* **2003**, *91*, 1785−1802.
(8) Salomon, A.; Cahen, D.; Lindsay, S.; Tomfohr, J.; Engelkes, V. B.; Frisbie, C. D. *Adv. Mater.* **2003**, *15*, 1881−1890.
(9) Zahid, F.; Paulsson, M.; Datta, S. Electrical Conduction through Molecules. In *Advanced Semiconductor and Organic Nano-Techniques*; Morkoc, H., Ed.; Academic Press: New York, 2003.
(10) Reed, M. A.; Zhou, C.; Muller, C. J.; Burgin, T. P.; Tour, J. M. *Science* **1997**, *278*, 252−254.
(11) Liang, W.; Shores, M. P.; Bockrath, M.; Long, J. R.; Park, H. *Nature* **2002**, *417*, 725−729.
(12) Magoga, M.; Joachim, C. *Phys. Rev. B* **1997**, *56*, 4722−4729.
(13) Bumm, L. A. *J. Phys. Chem. B* **1999**, *103*, 8122−8127.
(14) Cui, X. D.; Primak, A.; Zarate, X.; Tomfohr, J.; Sankey, O. F.; Moore, A. L.; Moore, T. A.; Gust, D.; Harris, G.; Lindsay, S. M. *Science* **2001**, *294*, 571−4.
(15) Oevering, H.; Paddon-Row: M. N.; Heppener, M.; Oliver, A. M.; Cotsaris, E.; Verhoeven, J. W.; Hush, N. S. *J. Am. Chem. Soc.* **1987**, *109*, 3258−3269.
(16) Schmidt, J. A.; Liu, J.-Y.; Bolton, J. R.; Archer, M. D.; Gadzekpo, V. P. Y. *J. Chem. Soc., Faraday Trans. 1* **1989**, *85*, 1027−1041.
(17) Davis, W. B.; Svec, W. A.; Ratner, M. A.; Wasielewski, M. R. *Nature* **1998**, *396*, 60−63.
(18) Piet, J. J.; Shuddeboom, W.; Wegewijs, B. R.; Grozema, F. C.; Warman, J. M. *J. Am. Chem. Soc.* **2001**, *123*, 5337−5347.
(19) Lukas, A. S.; Zhao, Y.; Miller, S. E.; Wasielewski, M. R. *J. Phys. Chem. B* **2002**, *106*, 1299−1306.
(20) Liu, R.; Holman, M. W.; Zang, L.; Adams, D. M. *J. Phys. Chem. A* **2003**, *107*, 6522−6526.
(21) Marcus, R. A.; Sutin, N. *Biochim. Biophys. Acta* **1985**, *811*, 265−322.
(22) Ulstrup, J.; Jortner, J. *J. Chem. Phys.* **1975**, *63*, 4358−4368.
(23) Closs, G. L.; Miller, J. R. *Science* **1988**, *240*, 440−7.
(24) Marcus, R. A. *Annu. Rev. Phys. Chem.* **1964**, *15*, 155−196.
(25) Xie, X. S. *Acc. Chem. Res.* **1996**, *29*, 598−606.
(26) Xie, X. S.; Trautman, J. K. *Annu. Rev. Phys. Chem.* **1998**, *49*, 441−480.
(27) van Hulst, N. F.; Veerman, J.-A.; García-Parajó, M. F.; Kuipers, L. *J. Chem. Phys.* **2000**, *112*, 7799−7810.
(28) Moerner, W. E. *J. Phys. Chem. B* **2002**, *106*, 910−927.

10.1021/ja047386o CCC: $27.50

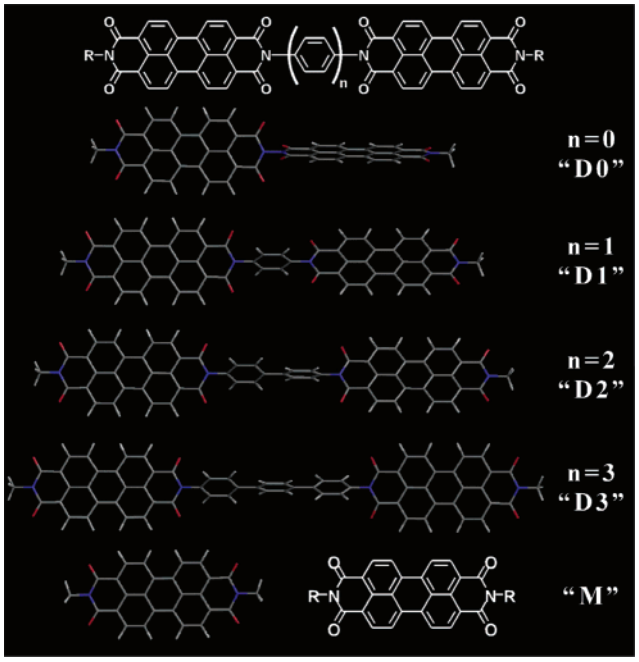

Figure 1. Structures of perylenebisimide dimers **D0**, **D1**, **D2**, and **D3**, and monomer **M**.

demonstrated that single-molecule fluorescence can be used to follow electron-transfer processes.[20,29−33] This fundamental chemical process of electron transfer is closely related to the process of electron transmission through a molecular wire, and indeed, relationships between the rate constant of electron transfer and the conductance have been proposed.[34−38] Spectroscopic studies of electron transfer can be thus designed to provide a useful tool in the effort to understand molecular electronic systems.

Here we demonstrate how the electronic properties and switching behavior of a prototypical symmetric donor−bridge−acceptor system can be comprehensively investigated by straightforward bulk optical investigations, theoretical modeling, ab initio quantum chemical calculations, and single-molecule spectroscopy. The dimer system studied here consists of perylenetetracarboxylbisimide end units connected via an oligo-1,4-phenylene bridge (*wire*) of adjustable length (Figure 1). These perylenebisimides are chromophores with strong absorption ($\epsilon \approx 80{,}000$), high fluorescence quantum yield ($\Phi_F \approx 1$),[39] and good photostability and chemical stability.[40]

(29) Holman, M. W.; Adams, D. M. *ChemPhysChem* **2004**, *5*, in press.
(30) Lu, H. P.; Xie, X. S. *J. Phys. Chem. B* **1997**, *101*, 2753−2757.
(31) Zang, L.; Liu, R.; Holman, M. W.; Nguyen, K. T.; Adams, D. M. *J. Am. Chem. Soc.* **2002**, *124*, 10640−10641.
(32) Holman, M. W.; Liu, R.; Adams, D. M. *J. Am. Chem. Soc.* **2003**, *125*, 12649−12654.
(33) Gronheid, R.; Stefan, A.; Cotlet, M.; Hofkens, J.; Qu, J.; Müllen, K.; Van der Auweraer, M.; Verhoeven, J. W.; DeSchryver, F. C. *Angew. Chem., Int. Ed.* **2003**, *42*, 4209−4214.
(34) Nitzan, A. *J. Phys. Chem. A* **2001**, *105*, 2677−2679.
(35) Mujica, V.; Nitzan, A.; Mao, Y.; Davis, W.; Kemp, M.; Roitberg, A.; Ratner, M. A. Electron Transfer in Molecules and Molecular Wires: Geometry Dependence, Coherent Transfer, and Control. In *Electron Transfer: From Isolated Molecules to Biomolecules*; Jortner, J., Bixon, M., Eds.; Advances in Chemical Physics Series 107; John Wiley & Sons: New York, 1999; pp 403−429.
(36) Nitzan, A. *Annu. Rev. Phys. Chem.* **2001**, *52*, 681−750.
(37) Nitzan, A. *Isr. J. Chem.* **2002**, *42*, 163−166.
(38) Creutz, C.; Brunschwig, B. S.; Sutin, N. Electron Transfer from the Molecular to the Nanoscale. In *Comprehensive Coordination Chemistry 2*; Fujita, M., Powell, A., Creutz, C. A., Eds.; Elsevier: Amsterdam, 2004; Vol. 7, pp 731−777.
(39) Kircher, T.; Löhmannsröben, H.-G. *Phys. Chem. Chem. Phys.* **1999**, *1*, 3987−3992.

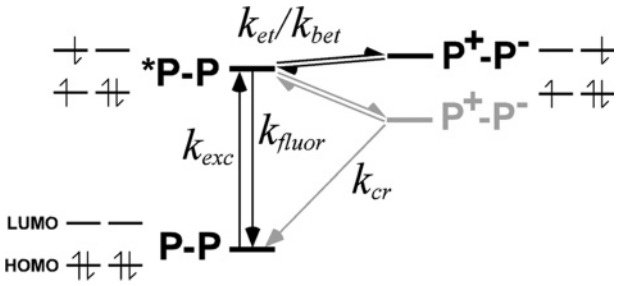

Figure 2. Energy levels and kinetic diagram for perylenebisimide dimers in nonpolar (black) and polar (gray) solvents.

Optical excitation of a perylenebisimide dimer (**P**−**P**) leads to creation of a singlet excited state (***P**−**P**) localized on one of the chromophores, which either radiatively decays to the ground state or undergoes IET to form a charge-separated state ($\mathbf{P}^+-\mathbf{P}^-$) (Figure 2). The charge-separated state is nonfluorescent, and thus, charge-transfer kinetics can be systematically studied by monitoring changes in the fluorescence. As we have noted previously for these molecules,[20] an increase in the solvent polarity leads to a decrease in the quantum yield of fluorescence by stabilizing the charge-separated state (gray pathway, Figure 2). As the driving force ($\Delta G°$) for electron transfer increases, k_{et} increases, becoming competitive with k_{fluor} (and shifting the equilibrium k_{et}/k_{bet} to the right), and less fluorescence is seen. By methodically varying both the molecular structure (Figure 1) and the environment while studying the fluorescence and fitting the resulting data, we determine key parameters such as the electronic coupling and seek to understand how factors such as bridge electronic structure and chromophore orientation affect these properties.

This switching of the electron transfer by changing the local environment also extends to the single-molecule level. Though molecules immobilized on surfaces or in polymer matrixes for SMS have electron-transfer behavior different from that of molecules in solution,[20] this behavior still depends critically on the local environment. Single-molecule techniques allow us to demonstrate not just that ensembles of identical molecules behave differently in different environments, but that the behavior of the same individual molecule can be changed, and changed reversibly, by altering the local environment.

Experimental Section

Symmetrically substituted perylene-3,4:9,10-tetracarboxylbisimide monomers (**M**) and symmetric perylene dimer systems (**D0**, **D1**, **D2**, and **D3**) (Figure 1) were synthesized as previously reported.[20] Bulky side groups R inhibit π-stacking and solubilize the perylenes to allow for facile synthesis and characterization, without affecting the spectroscopic properties of the chromophore. For **M** and **D0** R = 1-hexylheptyl, and for **D1**, **D2**, and **D3**, R = 1-nonyldecyl.

Solution absorption spectra were collected on a PerkinElmer Lambda 25 UV/vis spectrometer, and solution fluorescence spectra were collected on a PerkinElmer LS 55 luminescence spectrometer. Temperature-dependent data were collected using PerkinElmer water-jacketed cell holders attached to a ThermoNeslab circulator. Quantum yields were calculated using standard procedures,[41] relative to **M** (R = 1-hexylheptyl) in acetonitrile, which has $\Phi_F \approx 1$.[39] Fits of the quantum yield data were found using a least-squares fitting method in Origin 6.0. Picosecond time-resolved emission measurements were carried out

(40) Langhals, H. *Heterocycles* **1995**, *40*, 477−500.
(41) Lakowicz, J. R. *Principles of Fluorescence Spectroscopy*, 2nd ed.; Plenum Publishers: New York, 1999.

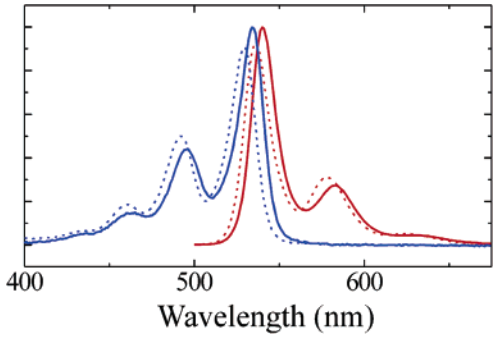

Figure 3. Absorption (blue solid line) and emission (red solid line) spectra of **D0** and absorption (blue dashed line) and emission (red dashed line) spectra of **D2**.

with a Hamamatsu streak camera, model C4334, optically coupled to a CCD array detector. A femtosecond laser pulse (100 fs) was generated from a mode-locked Ti−sapphire laser system pumped with a frequency-doubled Nd:YLF laser. The repetition rate was lowered to 1 kHz. The output centered at 800 nm was doubled through a BBO crystal to generate 400 nm light (1 nJ/pulse) that was used to excite the sample. Lifetime determinations were made from these data using Hamamatsu software HPD-TA32 (version 3.1.0).

For single-molecule measurements, molecules were sparsely distributed between ∼50 nm thin films of poly(vinyl acetate) (PVAc) or poly(vinyl alcohol) (PVAl) on clean glass cover slips by spin coating one drop of a solution of 2 mg/mL PVAc in $CHCl_3$ or of 2 mg/mL PVAl in 1.2% glycerol/water, followed by a drop of 4×10^{-10} M **D0** in $CHCl_3$, followed by another drop of polymer solution, all at 1500 rpm. Single-molecule fluorescence imaging and fluorescence trajectory collection were performed under an argon atmosphere, using a Digital Instruments Aurora 2 near-field scanning optical microscope modified to function as a scanning confocal microscope, equipped with a 100× 1.25 NA objective (Zeiss), a 488 nm holographic supernotch filter (ThermoOriel) to remove the excitation light, and single-photon-counting avalanche photodiode (APD) detectors (PerkinElmer/EG&G SPCM-AQR-15). The typical experiment involved continuous optical excitation with circularly polarized 488 nm light from an argon ion laser (Melles-Griot), focused to a diffraction-limited spot (fwhm ≈ 250 nm), leading to an excitation power at the sample of ∼500 W/cm^2, and collection of emitted photons at the APD with a 20 ms integration time.

Ab initio quantum chemical calculations of electron-transfer matrix elements[42,43] were performed using Jaguar 3.5[44] at the Hartree−Fock level of theory, using a 6-31G** basis set. The perylenebisimide geometry used was obtained from a full geometry optimization using density functional theory (DFT) at the B3LYP level with a 6-31G** basis set.

Results and Discussion

Dielectric Switching of Electron Transfer. Both absorption and fluorescence spectra of the dimers (Figure 3) are similar in shape and maxima to those of the corresponding perylenebisimide monomers under all conditions, implying that throughout these experiments fluorescence is from the locally excited state at one perylene unit. In nonpolar solvents, the free energy change ($\Delta G°$) for the electron-transfer reaction (k_{et}, Figure 2) is positive (black pathway, Figure 2), so k_{et} is slow relative to k_{fluor}, and the equilibrium k_{et}/k_{bet} lies to the left. Essentially, the molecule remains in the locally excited state (***P**−**P**), so the fluorescence

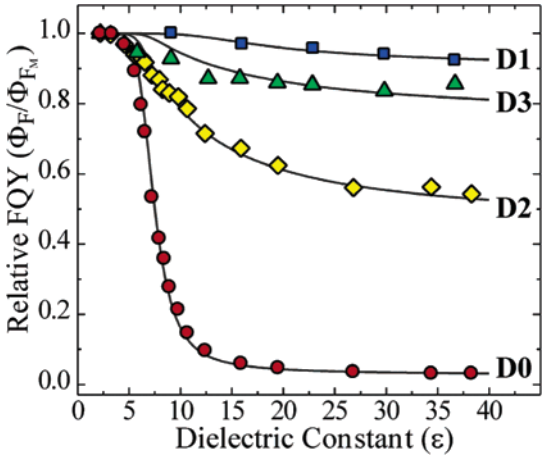

Figure 4. Fluorescence quantum yield relative to monomer fluorescence quantum yield for **D0** (●), **D1** (■), **D2** (◆), and **D3** (▲). The solid lines are fits using eqs 1−5 with $\lambda_i = 0.25$ eV, $h\nu = 1500$ cm^{-1}, $r = 5.5$ Å, $E_{ox} = 1.61$ V, $E_{red} = 0.59$ V, $\Delta G_{S_1-S_0} = 2.309$ eV, $\epsilon_{ref} = 36.64$ (acetonitrile), and the parameters shown in Table 1.

quantum yield is near unity, as in the monomer. In polar solvents, which are better able to stabilize the charge-separated state (**P**$^+$−**P**$^-$), $\Delta G°$ for electron transfer becomes negative, k_{et} becomes fast relative to k_{fluor}, and the equilibrium k_{et}/k_{bet} lies to the right. The molecule undergoes IET to form the charge-separated state (**P**$^+$−**P**$^-$) and remains there until nonradiative charge recombination (k_{cr}) returns it to the ground state, and the fluorescence is quenched. In solvents of intermediate polarity, $\Delta G°$ is close to zero, so the charge-separated state and the locally excited state are in equilibrium and the amount of fluorescence seen depends on the position of the equilibrium and the relative rates of k_{fluor} and k_{cr}.

The fluorescence quantum yield of each dimer relative to that of the monomer **M** (Φ_F/Φ_{FM}, relative Φ_F) in the same solvent or solvent mixture was collected across a broad range of solvent dielectric constants (ϵ) at room temperature for all four dimers (Figure 4). Under all conditions the quantum yield of the monomer (Φ_{FM}) was close to 1, so this correction is minor, but it does give more consistent results than using Φ_F alone. All of these data were taken in binary mixtures of 1,4-dioxane (dioxane) ($\epsilon = 2.21$) and *N*,*N*-dimethylformamide (DMF) ($\epsilon = 38.3$), but in general other solvents and solvent mixtures give a Φ_F/Φ_{FM} that is very similar to that found in the dioxane/DMF mixture of the same dielectric constant, suggesting that these changes in relative Φ_F are due primarily to the dielectric constant change, and that any solvent-specific effects are mostly factored out by using the relative Φ_F.

For all dimers, the relative Φ_F decreases with increasing dielectric constant, meaning that the frequency of electron transfer increases: k_{et} is faster, and the equilibrium k_{et}/k_{bet} lies further to the right, toward the charge-separated state (**P**$^+$−**P**$^-$). As expected, larger distances between chromophores leads to less electron transfer: $\Delta G°$ for charge separation will be larger, but more importantly, the electronic coupling ($\mathbf{H}_{AB}$) between the two chromophores is weaker, so k_{et} (and k_{cr}) will be slower and less competitive with k_{fluor}. This change is not uniform across the series, however: as expected, there is less electron transfer for **D1** than for **D0**, but for **D2** there is actually more electron transfer than for **D1**. We have observed this anomaly previously in solution and single-molecule fluorescence measurements,[20] and attributed it qualitatively to weaker electronic

(42) Zhang, L. Y.; Friesner, R. A.; Murphy, R. B. *J. Chem. Phys.* **1997**, *107*, 450−459.
(43) Baik, M.-H.; Crystal, J. B.; Friesner, R. A. *Inorg. Chem.* **2002**, *41*, 5926−5927.
(44) Jaguar 3.5, Schrödinger, Inc., Portland, OR, 1998.

Table 1. Center-to-center Distance d between the Two Chromophores in Each Dimer and the Values for $\mathbf{H}_{AB}$ and k_{cr} from the Fits Displayed in Figures 4 and 5

	D0	D1	D2	D3
d (nm)	1.29	1.72	2.16	2.59
		$T = 298$ K		
$\mathbf{H}_{AB}$ (cm^{-1})	97	19	51	34
k_{cr} (s^{-1})	7.5×10^8	1.0×10^6	5×10^9	5×10^8
		$T = 333$ K		
$\mathbf{H}_{AB}$ (cm^{-1})	97		45	
k_{cr} (s^{-1})	2.1×10^8		4×10^9	

coupling (smaller $\mathbf{H}_{AB}$) in **D1**. In this paper, $\mathbf{H}_{AB}$ and other parameters influencing IET and thus Φ_F are determined quantitatively, and the reasons for the trends and aberrations in these values are explored in greater detail.

Electron-Transfer Theory and Fitting of Dielectric Dependence. For each dimer molecule the data in Figure 4 are well-described by standard electron-transfer theory developed by Marcus[21,24] and elaborated by Jortner[22,45] and others,[23] along with some fairly simple solvation models.[15,46] The general equation developed by these authors[23] is

$$k_{et} = \frac{2\pi}{\hbar}\mathbf{H}_{AB}{}^2 \frac{1}{[4\pi\lambda_o k_b T]^{1/2}} \sum_{w=0}^{\infty} (e^{-S} S^w / w!) \times \exp\left(\frac{-(\lambda_o + \Delta G^\circ + wh\nu)^2}{4\lambda_o k_b T}\right) \quad (1)$$

where $\mathbf{H}_{AB}$ is the electronic coupling matrix element between the initial and final states, ΔG° is the free energy change for the electron-transfer reaction, and $h\nu$ is the energy of the molecular vibrational modes, taken here as 0.186 eV (=1500 cm^{-1}), since the carbon skeletal vibrations which are found near that energy are believed to be the most involved in electron transfer.[23,39] The term S represents the vibrational−electronic coupling strength and is equal to

$$S = \frac{\lambda_i}{h\nu} \quad (2)$$

where λ_i is the reorganization energy of the chromophore (the internal reorganization energy); $\lambda_i = 0.25$ eV, a value typical for large aromatics, is used, following previous studies on perylenebisimides.[39] The parameter λ_o is the solvent ("outer sphere") reorganization energy, given by

$$\lambda_o = \frac{\epsilon^2}{4\pi\epsilon_0}\left(\frac{1}{\epsilon_{op}} - \frac{1}{\epsilon}\right)\left(\frac{1}{r} - \frac{1}{d}\right) \quad (3)$$

where ϵ_{op} is the optical dielectric constant (=n^2, the square of the refractive index), which does not vary greatly ($\epsilon_{op} = 2.0232$ for dioxane and 2.0463 for DMF) over the solvent range used here and for which an average value of 2.0348 is used in the fitting; r is the electronic radius of the ions in question, and is taken as 0.55 nm, roughly the distance from the center of the perylenebisimide to the nitrogen atom at its edge, as the perylenebisimide HOMO and LUMO are found in electronic structure calculations to be delocalized over the entire π-system; and d is the center-to-center distance between the two chromophores, given in Table 1 for each dimer. This reorganization term increases with dielectric constant, which would lead to a decrease in electron-transfer rates, but the decrease in ΔG° with increasing dielectric constant overrides this effect and leads to an overall increase in k_{et}. The expression we use to calculate the change in ΔG° for electron transfer with dielectric is[15,46]

$$\Delta G^\circ = e(E_{ox} - E_{red}) - \Delta G_{S_1-S_0} + \frac{e^2}{4\pi\epsilon_0}\left[\left(\frac{1}{\epsilon}\right)\left(\frac{1}{r} - \frac{1}{d}\right) - \left(\frac{1}{\epsilon_{ref}}\right)\left(\frac{1}{r}\right)\right] \quad (4)$$

E_{ox} and E_{red} are the oxidation and reduction potentials of a perylenebisimide, 1.61 and −0.59 V, respectively, measured in acetonitrile;[39] $\Delta G_{S_1-S_0}$ is the energy of a single optical excitation, 2.31 eV, calculated from the absorption/emission spectra; ϵ, r, and d are as in eq 2; and ϵ_{ref} is the dielectric constant of acetonitrile, 36.64. This theoretical approach is of course somewhat simplified, but has been adopted here on the basis of its past successes,[15,23,39] and gives good fits to our data with reasonable values of key parameters.

Equation 1 is used to calculate both k_{et} and k_{bet} (cf. Figure 2); the parameters for calculated k_{bet} are the same as those for k_{et} save that the sign of ΔG° is reversed. A similar Marcus treatment could be used for k_{cr}, with parameters calculated similarly, though with a different $\mathbf{H}_{AB}$, but we find it simpler and more accurate to use a constant value for k_{cr} as a fitting parameter. The value of k_{cr} affects the observed Φ_F only in the relatively narrow range where k_{et} and k_{bet} are similar, and k_{cr} is expected to vary only slightly in this range. In addition, any other process that inhibits back electron transfer to the singlet locally excited state (k_{bet}), such as molecular reorganization (possibly to achieve a more decoupled "twisted" state[18,47]) or intersystem crossing to a triplet state, will have the same effect as charge recombination on the observed quantum yield, so "k_{cr}" may be a composite of rate constants for several processes. Our time-resolved fluorescence results (vide infra) suggest that the constant k_{cr} approach is basically valid here.

For a kinetic scheme like the one sketched in Figure 2, the fluorescence quantum yield is given by[48]

$$\Phi_F = \frac{k_{fluor}(k_{bet} + k_{cr})}{k_{fluor}(k_{bet} + k_{cr}) + k_{et}k_{cr}} \quad (5)$$

Using eqs 1−5, we find good fits to the Φ_F vs ϵ curve for each dimer, using only two adjustable parameters, $\mathbf{H}_{AB}$ and k_{cr}. The fits are shown as solid lines in Figure 4, and the parameters used are given in Table 1. The trends in both $\mathbf{H}_{AB}$ and k_{cr} follow the same pattern noted in the overall amount of fluorescence quenching: decreasing from **D0** to **D1** and then increasing for **D2**.

To test the reliability of our model and better understand the effects influencing the values of these parameters, the dimers **D0** and **D2** were also studied in the same series of dioxane−DMF solvent mixtures at 333 K. The results are shown in Figure 5, where they are compared to the data collected at 298 K (the same as those shown in Figure 4). The same model (eqs 1−5)

(45) Kestner, N. R.; Logan, J.; Jortner, J. *J. Phys. Chem.* **1974**, *78*, 2148−2166.
(46) Weller, A. *Z. Phys. Chem.* **1982**, *133*, 93−98.
(47) Rettig, W. *Angew. Chem., Int. Ed. Engl.* **1986**, *25*, 971−988.
(48) Poteau, X.; Brown, A. I.; Brown, R. G.; Holmes, C.; Matthew, D. *Dyes Pigm.* **2000**, *47*, 91−105.

Table 2. Time-Resolved Fluorescence Data for **D0** and **D2** and Calculated Electron-Transfer Rates

	D0				D2			
	dioxane	THF	DMF (15%)	DMF	dioxane	THF	DMF (15%)	DMF
ϵ	2.21	7.58	7.62	38.3	2.21	7.58	7.62	38.3
Φ_F	1.00	0.78	0.58	0.04	1.00	0.71	0.72	0.49
τ_1 (ns)	3.03	3.99	3.35	2.74	3.63	2.46	2.73	2.16
τ_2 (ns)		0.24	0.46	0.062		0.12	0.14	0.084
A_2/A_1		1.43	2.13	18.4		0.258	0.437	0.399
k_{et} (s^{-1})		2.14×10^9	1.19×10^9	1.67×10^{10}		1.68×10^9	2.06×10^9	3.43×10^9
k_{bet} (s^{-1})		1.76×10^9	6.50×10^8	7.59×10^8		6.10×10^9	4.71×10^9	7.82×10^9
k_{cr} (s^{-1})		1.37×10^8	2.39×10^8	4.41×10^8		6.17×10^8	3.86×10^8	8.21×10^8

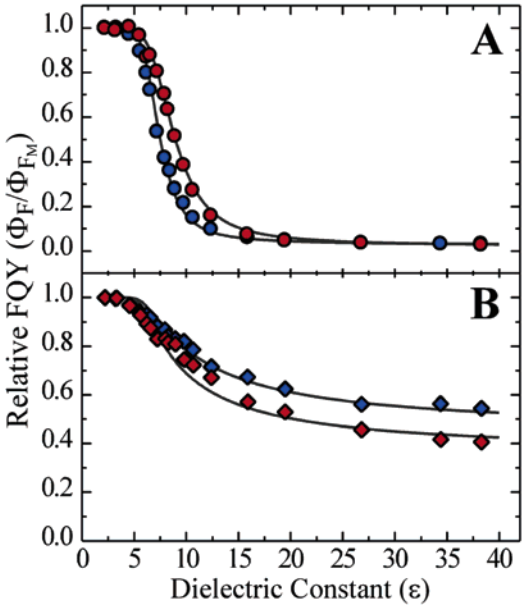

Figure 5. Relative quantum yield versus dielectric constant for (A) **D0** at 298 K (●) and 333 K (●) and (B) **D2** at 298 K (◆) and 333 K (◆). Solid lines are fits as in Figure 4, with parameters from Table 1.

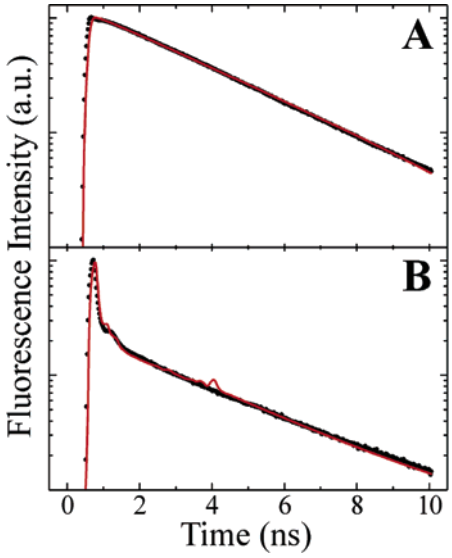

Figure 6. Sample time-resolved fluorescence data from **D0** in (A) dioxane ($\epsilon = 2.2$) and (B) DMF ($\epsilon = 38.3$). Solid lines are fits using eq 6 and the procedure described in the text, with the parameters in Table 2.

was also used to fit these high-temperature data; the values thus obtained are given in Table 1, and the fits are plotted (solid lines) in Figure 5. As it should, the model fits the data for **D0** with the same $\mathbf{H}_{AB}$ and a slightly lower k_{cr}. If k_{cr} for **D0** is predominantly governed by a Marcus-type relation, then it is expected that it would be slower at higher temperatures, since the estimated $\Delta G°$ for the charge-recombination reaction would place it well into the Marcus inverted region. For **D2** the result is similar, though a slightly different $\mathbf{H}_{AB}$ is required to give a good fit. It is plausible that the coupling in **D2** could be affected by temperature, since the coupling will depend on the interplanar angle between the two chromophores and in **D2** there are more, and less constrained, rotational degrees of freedom by which this interplanar angle could change.

To further corroborate this model, we also collected the time-resolved fluorescence of the dimers **D0** and **D2**, and, for comparison, the monomer **M** (R = 1-nonyldecyl), in several solvent mixtures. The fluorescence decay of the monomer is single-exponential, with a lifetime around 4 ns. For **D0** and **D2** in pure dioxane ($\epsilon = 2.21$) the decays were also single-exponential, with similar lifetimes (Figure 6A), indicting that, as expected from the quantum yield measurements, there is no appreciable IET for these dimers in nonpolar solvents. Time-resolved fluorescence of dimers in solvent mixtures of intermediate (tetrahydrofuran (THF), $\epsilon = 7.58$; 85:15 v/v dioxane: DMF, $\epsilon = 7.62$) and higher (pure DMF, $\epsilon = 38.3$) polarity shows biexponential kinetics with faster decay components that reflect the IET occurring from the excited state (Figure 6B).[48−50] The fluorescence intensity at any point in time is proportional to the concentration of the excited state ([***P**−**P**]), which is being depopulated by both the usual radiative decay (k_{fluor}) and intramolecular electron transfer (k_{et}), leading to biexponential behavior. For the kinetic scheme shown in Figure 2, the observed biexponential fluorescence decay

$$I_{fluor} \propto [^*\mathbf{P}{-}\mathbf{P}] = A_1 e^{-t/\tau_1} + A_2 e^{-t/\tau_2} \quad (6)$$

should be given by[48,51]

$$\frac{A_2}{A_1} = \frac{\frac{1}{\tau_1} - k_{fluor} - k_{et}}{k_{fluor} + k_{et} - \frac{1}{\tau_2}} \quad (7)$$

and

$$\frac{1}{\tau_{1,2}} = \frac{1}{2}[k_{fluor} + k_{et} + k_{bet} + k_{cr} \pm [(k_{bet} + k_{cr} - k_{fluor} - k_{et})^2 + 4k_{et}k_{bet}]^{1/2}] \quad (8)$$

The time-resolved fluorescence data are presented in Table 2.

(49) Heitele, H.; Pöllinger, F.; Häberle, T.; Michel-Beyerle, M. E.; Staab, H. A. *J. Phys. Chem.* **1994**, *98*, 7402−7410.
(50) Osuka, A.; Noya, G.; Taniguchi, S.; Okada, T.; Nishimura, Y.; Yamazaki, I.; Mataga, N. *Chem.—Eur. J.* **2000**, *6*, 33−46.
(51) Ware, W. R.; Watt, D.; Holmes, J. D. *J. Am. Chem. Soc.* **1974**, *96*, 7853−7860.

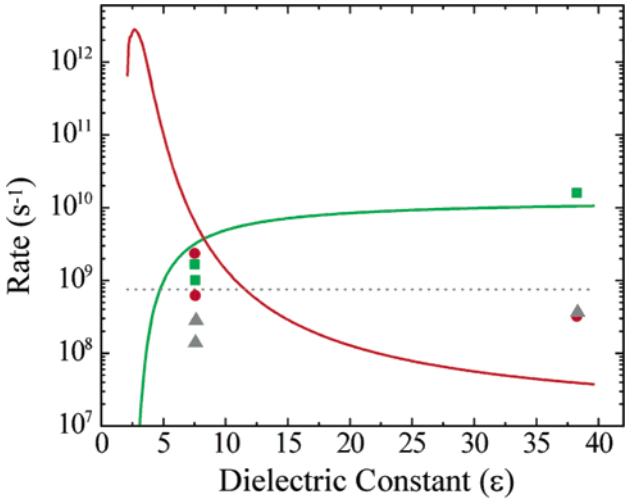

Figure 7. Electron-transfer rates k_{et} (green solid line), k_{bet} (red solid line), and k_{cr} (dotted line) for **D0**, as predicted by eqs 1−4 (using the same parameters from the fit in Figure 4) and measured rates k_{et} (green ■), k_{bet} (red ●), and k_{cr} (gray ▲) from time-resolved measurements using eqs 5−8.

Using these values along with the measured fluorescence quantum yield and eqs 5, 7, and 8, it is possible to calculate k_{et}, k_{bet}, and k_{cr} directly. The results also appear in Table 2, and a comparison of these experimentally determined rates for **D0** with the rates calculated by eqs 1−5 with the parameters in Table 1 is shown in Figure 7. The agreement between the model and the experiment is fairly good, given the relative simplicity of the model and the differences between the time-resolved experiment and the quantum yield measurements from which the modeled rates were derived. The largest deviations, as might be expected, are at high dielectric constant, where k_{et} is higher than both k_{fluor} and k_{bet}, and the quantum yield is more weakly dependent on the rates k_{bet} and k_{cr}. As can be seen in Table 2, the results for **D2** are less promising—k_{bet}, for instance, is higher at high dielectric—suggesting that, while the kinetic model shown in Figure 2 and presumed by eqs 5, 7, and 8, captures the quantum yield trends, it is only approximate for these larger dimers due to the involvement of the bridge.

Ab Initio Quantum Chemical Calculations of H_{AB}. We have also utilized an ab initio method available[42,43] for calculating the electronic coupling matrix element $\mathbf{H}_{AB}$, to see if the effects we have observed can be predicted and understood theoretically. This method calculates the full Hartee-Fock electronic structure of the donor and acceptor initial (Ψ_i) and final (Ψ_f) states and calculates the matrix element $\mathbf{H}_{AB}$ according to[43,52]

$$\mathbf{H}_{AB} = \frac{\int \Psi_i^* H \Psi_f - (\int \Psi_i^* \Psi_f)\int (\Psi_i^* H \Psi_i)}{1 - (\int \Psi_i^* \Psi_f)^2} \qquad (9)$$

Since the Hartree−Fock orbitals of the charge-separated state ($\mathbf{P}^{+-}\mathbf{P}^{-}$) that comprises the final state (Ψ_f) for a true intramolecular calculation were not readily obtained, we have used the intermolecular model systems shown in Figure 8A, in which the bridge is removed from the calculation and the two perylenebisimides are separated in space, either capped with hydrogen atoms (Figure 8A, top—*N*-(1-methyl)-*N*′-(hydro)-perylene-3,4:9,10-tetracarboxylbisimide or "MHP" model) or with the dangling-bond nitrogen changed to an oxygen to make the monoimide−monoanhydride (Figure 8A, bottom—*N*-(1-methyl)perylene-3,4:9,10-tetracarboxyl-3,4-anhydride-9,10-imide or "MPA" model). The perylene cation and anion wave functions were calculated separately and "stitched together" to form the final state (Ψ_f). The wave function of the photoexcited donor (***P**) is formed by promoting one electron from the HOMO to the LUMO of the ground-state wave function.

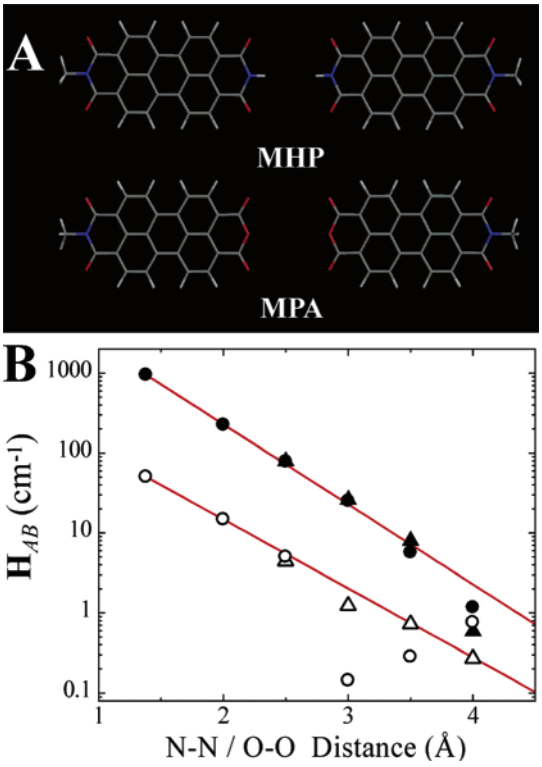

Figure 8. (A) Dimer models used in the $\mathbf{H}_{AB}$ calculation, with the perylenebisimides either capped with hydrogens (MHP model, top) or with the dangling-bond nitrogen changed to an oxygen to make the monoimide−monoanhydride (MPA model, bottom). (B) Calculated $\mathbf{H}_{AB}$ vs the distance separating the perylene:MHP model with the perylenes planar (▲) and orthogonal (△), and MPA model with the perylenes planar (●) and orthogonal (○). Open shapes are for orthogonal conformations, and closed shapes are for coplanar perylenes.

In Figure 8B the calculated $\mathbf{H}_{AB}$ values are plotted versus the edge-to-edge distance between the two chromophores (the N−N distance for the MHP model and the O−O distance for the MPA model). The expected exponential decay with distance is seen for both orthogonal (open shapes) and coplanar (filled shapes) conformations of the perylene, and both models give essentially the same results, though the smaller distances are accessible only in the MPA model. The values appear more scattered in the log plot at larger distances, since the coupling becomes negligible (less than the error in the calculation) by around 4 Å. At the separation expected for **D0**, roughly 1.38 Å, in the orthogonal alignment, which **D0** is expected to adopt, an $\mathbf{H}_{AB}$ value of 50.7 cm^{-1} is calculated, in reasonable agreement with the value of 97 cm^{-1} that was found from fitting the dielectric dependence data. Since the calculation does not include the covalent connection between the two chromophores, it is not surprising that the value from the calculation is somewhat lower. In addition, while a dihedral angle of 90° should be the minimum energy conformation for **D0**, the dimer

(52) Newton, M. D. *Chem. Rev.* **1991**, *91*, 767−792.

can probably access other dihedral angles, which may have higher coupling values. The effect on the average H_{AB} value should not be great, as the range of angles accessible is relatively narrow—between roughly 80° and 100°—and the H_{AB} values for those dihedrals are not dramatically different, in fact decreasing slightly (see the Supporting Information for details). The values calculated from these models for the larger dimers, however, are *much* lower—close to zero—indicating that in **D1**−**D3** the bridge is playing a larger role in mediating the electronic coupling.

These calculations indicate that, contrary to previous suggestions,[20] intrinsic favorability of the perpendicular conformations for electronic coupling cannot be the explanation for the unusual trends. The through-space electronic coupling is in fact stronger in coplanar systems, so the higher coupling in **D2** and **D3** must be related to some favorable interaction with the bridge. Though future calculations, incorporating the bridges in **D1**−**D3**, will help to explain the trends in H_{AB}, we speculate that higher coupling in **D2** and **D3** than in **D1** is due to the more accessible molecular orbitals in the bridge helping to mediate the electronic coupling between the two perylenebisimides. Molecular orbital calculations on the dimers **D1**−**D3**, using DFT at the B3LYP level with a 6-31G** basis set, indicate that the LUMO of the bridge (the lowest unoccupied orbital that is localized on the bridge) is at +0.063 eV for **D1**, −0.690 eV for **D2**, and −1.037 eV for **D3**. This change amounts to a lower barrier height between the two perylenebisimide LUMOs, and the resulting increased coupling could counteract the decrease in coupling expected from the increased distance. Similar explanations have been proposed for IET rate trends in other donor−bridge−acceptor systems.[17,53]

Single-Molecule Switching of Electron Transfer. When dispersed in thin films of poly(vinyl acetate) and examined in a scanning confocal microscope, single molecules of **M** exhibit bright fluorescence (50−150 counts/20 ms) and dimers (**D0**−**D3**) give approximately twice the fluorescence (100−300 counts/20 ms), indicating that there is no fast IET affecting Φ_F for the single molecules. Typical experiments involve raster scanning the sample to image an area and locate isolated molecules, and then collecting fluorescence traces—fluorescence intensity versus time—by positioning one molecule at a time over the laser spot. We have previously reported how slow IET and charge recombination can be observed in these single-molecule fluorescence traces,[31,32] and noted that the probability of IET occurring in the single molecules of **D0**−**D3** in a polymer follows the same trend as the quantum yields in solution.[20]

Following the logic of the solution experiments, we attempted to "switch" the IET of **D0** by modulating the local environment. We carried out single-molecule fluorescence measurements for **D0** embedded in a polymer matrix, where the molecules were trapped between two thin films (~50 nm each) of PVAc. The rigid environment of the PVAc slows electron transfer by increasing the reorganization energy (λ_o) and by limiting conformational change that could stabilize the charge-separated state ($\mathbf{P}^+-\mathbf{P}^-$), keeping $\Delta G°$ positive. Thus, for most molecules, strong fluorescence with the two perylene chromophores photobleaching sequentially ("two-step" behavior, like that shown in Figure 9A) was observed. Some molecules, however, find a conformation and/or nanoenvironment for which IET is favorable, so in these cases erratic "blinky" traces with no stable fluorescence levels (Figure 9B) are seen, since the IET leads to fluctuations in fluorescence intensity (blinking) on time scales faster than the time resolution of the experiment (20 ms). A fluorescence image of molecules of **D0** in PVAc is displayed in Figure 10A. Most molecules show strong, steady fluorescence, but a few blinks can be seen as dark pixels or lines. When **D0** is placed in a still more polar polymer environment, between layers of PVAl, where the charge-separated state can be better stabilized and $\Delta G°$ becomes close to zero or negative, such erratic blinking behavior is more common, and the fluoresence may be weaker due to quenching by rapid IET. In addition, irreversible photobleaching (possibly via a reaction

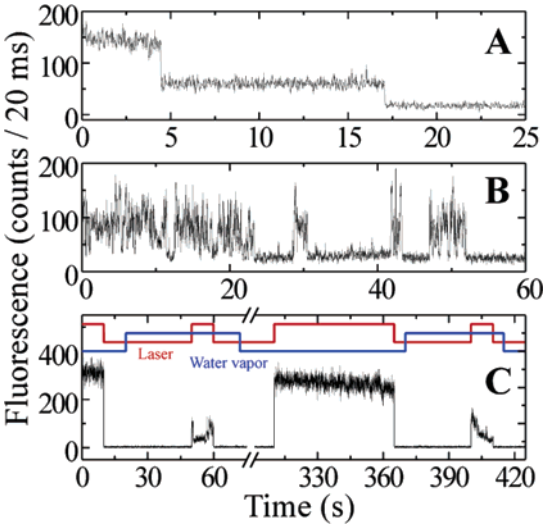

Figure 9. Dimer single-molecule fluorescence trajectories showing (A) two-step behavior with no blinking or (B) rapid, unresolved blinking due to IET and (C) demonstrating the effect of changing the local dielectric constant with water vapor.

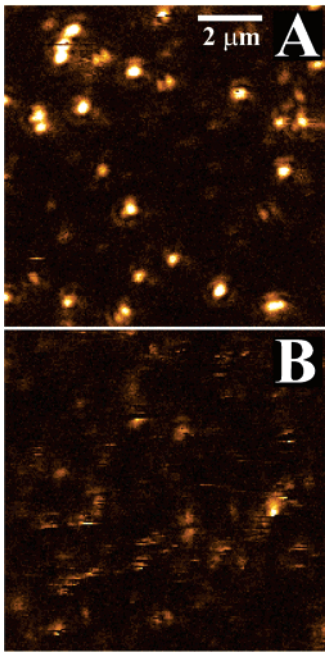

Figure 10. Fluorescence images of **D0** inside films of (A) poly(vinyl acetate) and (B) poly(vinyl alcohol). Raster scanning is from left to right, top to bottom.

(53) Kilså, K.; Kajanus, J.; Macpherson, A. N.; Mårtensson, J.; Albinsson, B. *J. Am. Chem. Soc.* **2001**, *123*, 3069−3080.

of the charge-separated state) happens quickly, so it is difficult to image the molecules or collect traces. Figure 10B shows an image of molecules of **D0** in PVAl; fluorescence intensities are lower, almost all molecules fluoresce erratically, and several disappear midscan.

We have found that it is possible to switch the IET on and off in the same single molecule within the same experiment, by altering the polymer environment with water vapor. Dry argon is normally blown over the sample throughout a single-molecule experiment, but when the argon is passed through a bubbler containing distilled water before reaching the sample, steady strong single-molecule fluorescence like that in Figure 9A changes to weaker, erratic fluorescence like that in Figure 9B, as illustrated in Figure 9C. As water molecules adsorb onto the surface and infiltrate the polymer, they can help stabilize the charge-separated state, decreasing $\Delta G°$ for IET, and they may also serve to partially solvate and loosen up the polymer, decreasing the reorganization energy and allowing the functional groups of the polymer to reorient more easily to stabilize the charge-separated state as well. This effect is reversible: if the water is removed and dry argon is blown over the sample for several minutes (while the laser is blocked, so that the molecule does not photobleach), the adsorbed water is driven off, and the stable, high-intensity fluorescence returns. Single-molecule spectroscopy provides for direct monitoring of electron-transfer switching behavior of the molecular wires, allowing for an alternative characterization method for molecular electronic materials, where the ultimate goal is to fabricate a *single-molecule* device.

Conclusions

We have used fluorescence spectroscopy of perylenebisimide dimers to evaluate the molecule wire behavior of a series of oligo-1,4-phenylene bridges. Since photoinduced intramolecular electron transfer quenches the fluorescence of the perylenebisimide chromophore, the electron-transfer behavior can be followed under various conditions by studying the fluorescence. By changing the solvent dielectric constant to vary $\Delta G°$ of electron transfer, and fitting the resulting curves using Marcus/Jortner theory, we can determine the electronic coupling between the two chromophores through the various bridges. Temperature-dependent and time-resolved measurements help to corroborate the models used in the fitting, but in the case of the larger dimers (**D2**, **D3**) indicate that other processes may be involved in charge recombination. Ab initio quantum chemical calculations of electronic coupling matrix elements give reasonable results for **D0**, but do not capture the bridge effects that seem to be crucial for understanding the coupling in **D1**−**D3**. Studies on new perylenebisimide dimers and more detailed quantum chemical calculations are under way and will help us to further refine our understanding of the factors controlling electron transfer through these bridges.

We have also shown that the study and control of these environmental effects on electron transfer can be extended to the single-molecule level. We are able to turn on and off electron transfer in isolated single molecules of **D0** in a polymer matrix by blowing wet and dry argon over the surface. The importance of single-molecule electron-transfer measurements and these environmental effects will only grow as the study of molecular electronic systems progresses, and future experiments along these lines will also help develop our understanding of these systems.

Acknowledgment. We thank Dr. John Miller and Dr. Marshall Newton for helpful discussions, Veeco/Thermomicroscopes and Dr. Stefan Kämmer for collaborations on instrument development, Prof. Mu-Hyun Baik, Lei Zhang, and Prof. Richard Friesner for assistance with and helpful discussions of electronic structure calculations, and Prof. Daniel Akins for time-resolved fluorescence measurements. This work was supported by the DOE under the award Agency Project No. DE-FG02-02ER15375 and partially by NSF MSREC Grant DMR-98-09687. D.M.A. thanks the Research Corp. for a Cottrell Scholar award, RC#CS0937.

Supporting Information Available: Figure showing the rotational potential for **D0** and calculated rotational dependence of $\mathbf{H}_{AB}$ at the **D0** distance (PDF). This material is available free of charge via the Internet at http://pubs.acs.org.

JA047386O